Design optimization of a Delta-like parallel robot through global stiffness performance evaluation

Eric Courteille, Dominique Deblaise, Patrick Maurine

Design Optimization of Robot Manipulators over Global Stiffness Performance Evaluation

Eric Courteille, Dominique Deblaise, Patrick Maurine

Abstract— **This paper presents a general framework for the design optimization of robot manipulators with respect to multiple global stiffness objectives. For this purpose, a systematic elasto-geometrical modeling method is used to derive the analytical manipulator stiffness models by taking into account their link and joint compliances. The models are then involved within an optimization process that is performed under a constraint of mass by using three global indices that describe the structure stiffness over the workspace. Multi-Objective Genetic Algorithm, i.e. Pareto-optimization, is taken as the appropriate framework for the definition and the solution of the addressed multi-objective optimization problem. Our approach is original in the sense that it is systematic and it can be applied to any serial and parallel manipulators for which stiffness is a critical issue.**

I. Introduction

The main objective for the mechanical design of robot manipulators consists in finding the best compromise between several properties, such as workspace, dexterity, manipulability, and stiffness [1]. Stiffness is an important issue for serial and parallel robots manipulators since their structures are now gradually being implemented to carry out various applications in fields such as medical, flight simulation and high-speed machining [2]. To make these machines compatible with their applications, it is necessary to model, identify and compensate all the effects that degrade their accuracy. These effects may be caused by errors in the geometry tolerances of the structure associated with machining and assembly errors of the various constituting bodies, and also by the elastic deformations of their structure [3]–[6]. The main problem is that a low stiffness of links and/or joints may lead to large compliant displacements of the end-effector under both structure own weight and external wrench applied at the end-effector [7]. These compliant displacements detrimentally affect both accuracy and payload performances, as pointed out for example in [8]. It is also to be noted that insufficient stiffness may induce low natural frequencies of the structure that lead to longer stabilization times and reduced dynamic performances [9] .

In the literature many efforts were recently devoted to the design optimization of robot manipulators by considering many competing objectives such as velocity transmission, workspace, inertia and stiffness [10]–[12]. These studies have shown the real efficiency of the evolutionary algorithms to solve this kind of problems. However, most of them do not include the analysis of the optimization results as part of the design process.

It is in this context that the presented work takes place. Our main objective is to fulfill the industrial demands in the preliminary design of the robots manipulators by optimizing simultaneously the stiffness over a specific workspace and/or by minimizing the global weight of the structure for increased dynamic performances, the whole in an acceptable timeframe. The main originality of our work resides :

- in a systematic analytical calculation of the equivalent stiffness matrix of the manipulator structures through a method that we proposed and experimentally validated in [13], [6],
- in the use of realistic global stiffness indices derived from the concatenation of the equivalent stiffness matrices locally calculated in the manipulator workvolume [14], [7],
- in the fact to provide an interactive use of Multi-Objective Genetic Algorithms (MOGA) in the robot design optimization as a reliable tool from an engineer point of view.

The paper is organized as follows. The stiffness modeling of a 3 degree-of-freedom translational parallel manipulator that is used to illustrate the proposed method is described first. The definition of local stiffness performance indices is done next. Global performance indices are then proposed and a sensitivity study is presented to show the coherence with the static positioning accuracy expected over the workspace. Then a practical application of the multi-objective optimization procedure is presented in order to define optimal stiffness designs of the studied structure for which the optimization results are carefully analyzed.

II. Stiffness modeling of a Delta like mechanism

The Surgiscope®[1] is a hybrid structure with a position mechanism based on a Delta like parallel manipulator [15] and a decoupled orientation mechanism. This structure is used in neurosurgery to move and to place accurately a microscope, a laser guiding system and some others surgical tools. In the following, the Surgiscope will only designate the position mechanism (Fig. 1).

The analytical stiffness model presented in this section is based on matrix structural analysis and has been introduced

E. Courteille, D. Deblaise, P. Maurine are with the LGCGM (EA 3913), Rennes, France and with the Department of Mechanical and Control Systems Engineering, INSA de Rennes, France
eric.courteille@insa-rennes.fr
dominique.deblaise@insa-rennes.fr
patrick.maurine@insa-rennes.fr

[1]ISIS: Intelligent Surgical Instrument & Systems http://www.isis-robotics.com/

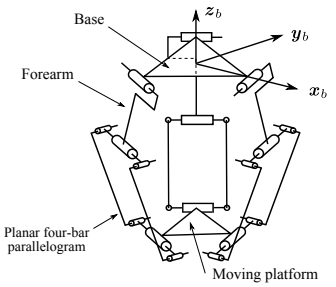

Fig. 1. The Surgiscope.

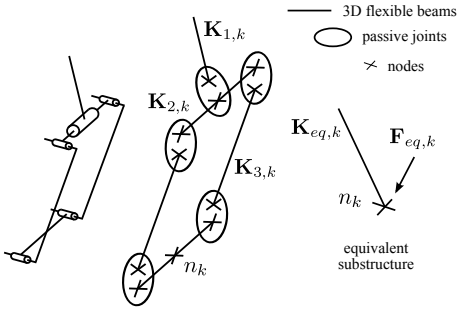

Fig. 2. Modeling of the k^{th} kinematic chain.

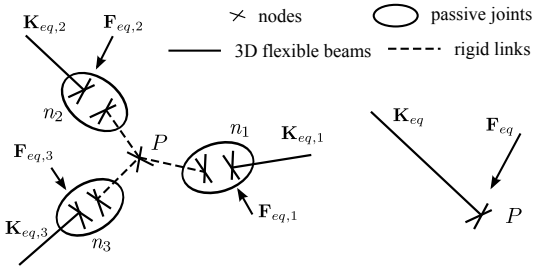

Fig. 3. Modeling of the equivalent structure.

in previous papers [13], [6]. Compared to traditional CAD-FEA approach, this analytical modeling leads both to a realistic stiffness description as well as a reduction of computational time that allows its use in a parametric optimization loop.

The stiffness modeling of the Surgiscope is composed with nodes corresponding to the characteristic points. These nodes link some 3D flexible beams, some rigid elements and some joints. The 6 dimensional equivalent stiffness matrix $\mathbf{K}_{eq}$ of the Surgiscope is defined in two steps as follows:

- definition of the equivalent substructure of each kinematic chain k ($k = 1, 2, 3$) defined by the equivalent stiffness matrix $\mathbf{K}_{eq,k}$ and the equivalent external wrench $\mathbf{F}_{eq,k}$ (Fig.2);
- assembly of the three equivalent kinematic chains to the moving platform considered as rigid. Definition of the equivalent structure defined by the stiffness matrix $\mathbf{K}_{eq}$ and the equivalent external wrench $\mathbf{F}_{eq}$ acting at the center point of the moving platform (Fig.3).

This stiffness modeling leads to the stiffness relation

$$\mathbf{F}_{eq} = \mathbf{K}_{eq}\, \Delta\mathbf{X}. \tag{1}$$

It is to be noted that the stiffness matrix $\mathbf{K}_{eq}$ depends on the geometrical parameters of each part of a kinematic chain. These parameters which will be optimized thereafter are defined in Table I.

1) Equivalent translational stiffness matrix: Relation (1) can be rewritten as

$$\begin{bmatrix} \mathbf{F} \\ \mathbf{M} \end{bmatrix} = \begin{bmatrix} \mathbf{K}_{11} & \mathbf{K}_{12} \\ \mathbf{K}_{21} & \mathbf{K}_{22} \end{bmatrix} \begin{bmatrix} \delta\mathbf{X} \\ \delta\mathbf{R} \end{bmatrix} \tag{2}$$

where $\mathbf{F}$ and $\mathbf{M}$ are respectively the equivalent external force and moment, the matrices $\mathbf{K}_{ij}$ defined a partition of the stiffness matrix $\mathbf{K}_{eq}$, $\delta\mathbf{X}$ and $\delta\mathbf{R}$ are respectively the translational and the rotational elastic displacements. Relation (2) can be rewritten as

$$\mathbf{F}^t_{eq} = \mathbf{K}^t_{eq}\, \delta\mathbf{X} \tag{3}$$

where $\mathbf{K}^t_{eq} = \mathbf{K}_{11} - \mathbf{K}_{12}\, {\mathbf{K}_{22}}^{-1}\, \mathbf{K}_{21}$ is the equivalent translational stiffness matrix and $\mathbf{F}^t_{eq} = \mathbf{F} - \mathbf{K}_{12}\, {\mathbf{K}_{22}}^{-1}\, \mathbf{M}$ is the equivalent external force which generates the translational elastic displacements $\delta\mathbf{X}$. It is to be noted that $\mathbf{F}^t_{eq}$ depends on the external moment $\mathbf{M}$.

2) Equivalent rotational stiffness matrix: Relation (2) is also used to defined the rotational stiffness relation

$$\mathbf{M}^r_{eq} = \mathbf{K}^r_{eq}\, \delta\mathbf{R} \tag{4}$$

where $\mathbf{K}^r_{eq} = \mathbf{K}_{22} - \mathbf{K}_{21}\, {\mathbf{K}_{11}}^{-1}\, \mathbf{K}_{12}$ is the equivalent rotational stiffness matrix and $\mathbf{M}^r_{eq} = \mathbf{M} - \mathbf{K}_{21}\, {\mathbf{K}_{11}}^{-1}\, \mathbf{F}$ is the equivalent external moment (depending on the external force $\mathbf{F}$) which generates the rotational elastic displacements $\delta\mathbf{R}$.

III. Stiffness performance evaluation

As explained in the previous section, at the static equilibrium and for a configuration in space i related to the actuator joint values $\mathbf{q}_i$, one can write the relation

$$\mathbf{F}_{eq,i} = \mathbf{K}_{eq,i} \Delta\mathbf{X}_i. \tag{5}$$

Since it has been shown in the previous part that this configuration-dependent Cartesian stiffness matrix $\mathbf{K}_{eq,i}$ can be obtained analytically, the stiffness performance of a manipulator can be studied in a systematic way. By the way, our goal is to propose in the following some possible indices to study the stiffness of robots manipulators. The approach we used is similar to those developed in the works related

TABLE I
PARAMETERS SUBJECT TO OPTIMIZATION

	Forearm	Parallelogram	
		long side	small side
Length (m)	L_1	L_2	L_3
Diameter (m)	ϕ_1	ϕ_2	ϕ_3
Thickness (m)	T_1	T_2	/

to the study of the manipulability of robot manipulators as well as the observability study of their geometrical errors and their geometrical calibration ([14], [16]–[20]). In the following, three local indexes are defined in order to describe the stiffness of the manipulator at a given configuration in space and three global indices are used to express its stiffness performance in the overall workspace.

A. Local stiffness indices

1) Volume of the local stiffness ellipsoid: A first stiffness index can be calculated by assuming that for a configuration i the elastic displacements $\Delta\mathbf{X}_i$ are bounded. As a result, the related force that is applied on the TCP $\mathbf{F}_{eq,i}$ is also bounded. Since the relation (5) is linear, the value of the elastic displacement bound can be chosen arbitrarily and it is usual to take its value so that:

$$\|\Delta\mathbf{X}_i\| \leq 1. \tag{6}$$

By substituting the bound value of $\Delta\mathbf{X}_i$ into (5) it comes:

$$\mathbf{F}_{eq,i}^T \left(\mathbf{K}_{eq,i}\mathbf{K}_{eq,i}^T\right)^{-1} \mathbf{F}_{eq,i} \leq 1. \tag{7}$$

As a result, if the Euclidian norm is used to describe the value of $\Delta\mathbf{X}_i$ bound in (6), the relation (5) maps the hypersphere in the space of the elastic displacements into an hyperellipsoid in the generalized force (wrench) space. The lengths of this hyperellipsoid semi-half-axes are the values of the eigenvalues of $\left(\mathbf{K}_{eq,i}\mathbf{K}_{eq,i}^T\right)^{-1}$ which are in fact the singular values of $\mathbf{K}_{eq,i}$ (Fig. 4). The singular values $\sigma_{j,i}$ $(j = 1, ..., 6)$ can be obtained through a Singular Value Decomposition (SVD) of $\mathbf{K}_{eq,i}$ according to:

$$\mathbf{F}_{eq,i} = \mathbf{K}_{eq,i}\Delta\mathbf{X}_i = \left(\mathbf{U}_i\mathbf{\Sigma}_{eq,i}\mathbf{V}_i^T\right)\Delta\mathbf{X}_i \tag{8}$$

The matrices $\mathbf{U}_i$ and $\mathbf{V}_i$ are orthogonal and $\mathbf{\Sigma}_{eq,i}$ is made up of the ordered singular values of $\mathbf{K}_{eq,i}$ in its main diagonal: $\mathbf{\Sigma}_{eq,i} = diag\left(\sigma_{1,i}, \cdots, \sigma_{6,i}\right)$ with $\sigma_{1,i} > \cdots > \sigma_{6,i}$.

The singular values $\sigma_{j,i}$ give an idea of the stiffness hyperellipsoid size and shape as well as an image of the amplification factor between respectively the elastic displacement and equivalent force spaces along the directions given by the eigenvectors of $\left(\mathbf{K}_{eq,i}\mathbf{K}_{eq,i}^T\right)^{-1}$. And for a manipulator configuration i, the bounds of $\Delta\mathbf{X}_i$ and $\mathbf{F}_{eq,i}$ are linked by:

$$\sigma_{6,i} \leq \frac{\|\mathbf{F}_{eq,i}\|}{\|\Delta\mathbf{X}_i\|} \leq \sigma_{1,i}. \tag{9}$$

As a result, the first index that can be defined to study the manipulator stiffness at the configuration i is given by:

$$S_{1,i} = \sqrt{\det\left(\mathbf{K}_{eq,i}^T\mathbf{K}_{eq,i}\right)} = \prod_{j=1}^{6}\sigma_{j,i}. \tag{10}$$

$S_{1,i}$ is related to the volume of the stiffness hyperellipsoid and the geometrical rationale that is behind this index is to make the volume of the stiffness hyperellipsoid as big as possible for the manipulator configuration i.

Let us note however that the calculation of $S_{1,i}$ which is based on the matrix $\mathbf{K}_{eq,i}$ that is not homogeneous in terms of units is not invariant with respects to those units [14], [7].

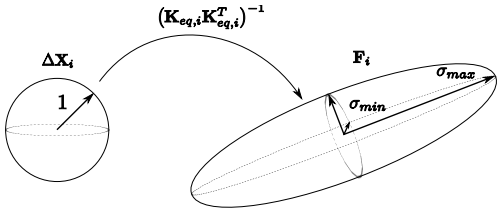

Fig. 4. Mapping between elastic displacement and force spaces.

One solution that can be used to overcome this problem is to split the matrix into its equivalent translational and rotational parts respectively $\mathbf{K}_{eq,i}^t$, $\mathbf{K}_{eq,i}^r$ defined in II-.1, II-.2 and to define subindexes related to each of them.

2) Condition number of the local stiffness matrix: A second possible index is the condition number of the stiffness matrix given by to the ratio of the maximum and minimum singular values of $\mathbf{K}_{eq,i}$:

$$S_{2,i} = \frac{\sigma_{max,i}}{\sigma_{min,i}} = \frac{\sigma_{1,i}}{\sigma_{6,i}}. \tag{11}$$

For a manipulator configuration i, the variations of the bounds of $\Delta\mathbf{X}_i$ and $\mathbf{F}_{eq,i}$ are linked by [21]:

$$\frac{\|\delta\Delta\mathbf{X}_i\|}{\|\Delta\mathbf{X}_i\|} \leq \frac{\sigma_{1,i}}{\sigma_{6,i}}\frac{\|\delta\mathbf{F}_{eq,i}\|}{\|\mathbf{F}_{eq,i}\|}. \tag{12}$$

Geometrically, the ratio $\frac{\sigma_{max,i}}{\sigma_{min,i}}$ gives an indication of the excentricity of the stiffness hyperellipsoid rather than its volume as it was the case with the previous index $S_{1,i}$. For minimum values of $S_{2,i}$ that is to say for values near to 1, this hyperellipsoid is closer to an hypersphere. As a result, minimizing this index allows to avoid for a manipulator configuration i a sharp stiffness ellispoid for which, the manipulator would have a high stiffness along a given axis and a low stiffness along an other.

As with the previous index $S_{1,i}$, since $\mathbf{K}_{eq,i}$ is not homogeneous, the value of $S_{2,i}$ will change according to the choice of unit. A possible solution of this problem is the definition of a dimensionless or dimensionally consistent stiffness matrix by dividing the rotational elements of $\mathbf{K}_{eq,i}$ by a characteristic length L that can be the length of the manipulator variable links in its nominal position of the *natural length* that minimizes the condition number for a reference pose [22], [23].

3) Minimum singular value of the local stiffness matrix: As the inequality (9) can be rewritten as:

$$\|\mathbf{F}_{eq,i}\| \geq \sigma_{6,i}\|\Delta\mathbf{X}_i\| \tag{13}$$

the greater is the minimum singular value $\sigma_{6,i}$, the greater is $\|\mathbf{F}_{eq,i}\|$ and thus the greater is the stiffness of the manipulator at configuration i. As a result a third possible stiffness index is defined as:

$$S_{3,i} = \sigma_{6,i}. \tag{14}$$

From a geometrical point of view, the index $S_{3,i}$ conveys the idea that for the configuration i, the shortest semiaxis of the stiffness hyperellipsoid should be as long as possible.

B. Global stiffness indices

Based upon the previously defined local indices, the three global stiffness indices that will be used further for the optimal design of manipulators are defined in an original manner [7]. For this purpose, the manipulator workspace is as usual discretized by using a regular space grid and for each equally spaced node N_i of the grid $(i = 1, ..., n_N)$, the equivalent stiffness matrix $\mathbf{K}_{eq,i}$ is calculated as well as its determinant in order to verify that the configuration related to the chosen node N_i is not singular. Then the global equivalent stiffness matrix $\mathbf{K}_{eq}^G$ is defined by the concatenation of all the n_N non-singular equivalent stiffness matrices $\mathbf{K}_{eq,i}$ as follows:

$$\mathbf{K}_{eq}^G = \begin{bmatrix} \mathbf{K}_{eq,1} \\ \mathbf{K}_{eq,2} \\ \vdots \\ \mathbf{K}_{eq,n_N} \end{bmatrix}_{(6n_N \times 6)} . \tag{15}$$

This global matrix links the global vector $\mathbf{F}^G$ of all resulting wrenches acting on the TCP at each node N_i for a given (6×1) generalized vector of TCP cartesian displacements $\Delta\mathbf{X}^G$:

$$\mathbf{F}^G = \mathbf{K}_{eq}^G \Delta\mathbf{X}^G. \tag{16}$$

From the definition of the global matrix $\mathbf{K}_{eq}^G$ and by using the same approach as the one used for the definition of the local stiffness indices, the three global stiffness indices are calculated as explained in the following.

1) Volume of the global stiffness ellipsoid: The first global stiffness index S_1 is related to the volume of the global stiffness ellipsoid which as to be maximized overall the manipulator workspace. Its value is calculated according the relation:

$$S_1 = \sqrt{\det\left(\mathbf{K}_{eq}^{GT}\mathbf{K}_{eq}^G\right)} = \prod_{j=1}^{6} \sigma_j^G \tag{17}$$

where ${\sigma_j}^G$ are the singular values obtained through the SVD of the $\mathbf{K}_{eq}^G$ as follows:

$$\mathbf{F}^G = \mathbf{K}^G \Delta\mathbf{X}^G = \left(\mathbf{U}^G \mathbf{\Sigma}^G {\mathbf{V}^G}^T\right) \Delta\mathbf{X}^G \tag{18}$$

with $\mathbf{\Sigma}^G = diag\left(\sigma_1^G, \cdots, \sigma_6^G\right)$ and $\sigma_1^G > \cdots > \sigma_6^G$.

2) Condition number of the global stiffness matrix: The second global stiffness index S_2 gives an indication of the excentricity of the global stiffness ellipsoid which as to be minimized overall the manipulator workspace. Its value is calculated according as follows:

$$S_2 = \frac{\sigma_{max}^G}{\sigma_{min}^G} = \frac{\sigma_1^G}{\sigma_6^G}. \tag{19}$$

3) Minimum singular value of the global stiffness matrix: The third global stiffness index S_3 concerns the length of the smallest semiaxis of the global stiffness ellipsoid which as to be maximized:

$$S_3 = \sigma_6^G. \tag{20}$$

IV. Surgiscope stiffness analysis

A. Calculation of the local and global stiffness indices of the Surgiscope

For the calculation of all indices, the workspace is discretized by using a regular spatial grid included in a singularity free area of the Surgiscope [24]. This grid is made of some parallel and horizontal planar grids defined within a volume described by $-0.3\,m \leq X \leq 0.3\,m$, $-0.3\,m \leq Y \leq 0.3\,m$ and $-1.4\,m \leq Z \leq 0.9\,m$.

In an attempt to solve the optimization problem in an acceptable timeframe while maintaining a smooth variation of the local stiffness indices from one node to the nodes that it is connected with, a number $n_N = 294$ nodes are regularly fixed over the Surgiscope workspace. This includes 6 planes of 49 nodes each. For all nodes, the 3×3 equivalent translational stiffness matrix $\mathbf{K}_{eq}^t$ (II-.1) is calculated in order to derive both the local $S_{1,i}$, $S_{2,i}$, $S_{3,i}$ and global S_1, S_2, S_3 stiffness indices previously described. Based upon this calculation, a qualitative analysis of the TCP elastic displacements and local stiffness indices is done a well as a study of the influence of the Delta geometrical parameter variations onto the Surgiscope global stiffness.

B. Qualitative Analysis between the TCP elastic displacements and local stiffness indices

This qualitative analysis is done in order to study the relation that exists between the variations of the TCP elastic displacements values and the variations of the related local stiffness indices. For this purpose, an horizontal planar grid is used at a given altitude within the Surgiscope workspace. For each node i of that grid, the equivalent translation stiffness matrix $\mathbf{K}_{eq}^t$ is calculated as well as the local stiffness indices $S_{1,i}$, $S_{2,i}$, $S_{3,i}$. By considering then a translational equivalent wrench $\mathbf{F}_{eq,i}^t = \begin{bmatrix} F_{x,i} & F_{y,i} & F_{z,i} \end{bmatrix}^T$ applied on the TCP, the translational elastic displacements δx_i, δy_i, δz_i are calculated and plotted with the local stiffness indices.

Fig. 5 gives an example of results for a 625 node grid set in the workspace at the altitude $Z = -1.2\,m$ which XY dimensions are given in IV-A when the constant wrench $\mathbf{F}_{eq,i}^t = \begin{bmatrix} 0 & 0 & -800 \end{bmatrix}^T\ (N)$ is applied at the TCP. This wrench describes the in use maximum load of the surgiscope. As one can see, the resulting TCP elastic displacements δz_i are minimum at the center of the grid ($\delta z_{min} = 1.2\,mm$) and they increase from 0 to more that 100% when the distance from the center rises to reach the borders of the grid ($\delta z_{max} = 2.5\,mm$). In a meantime, the local stiffness indices $S_{1,i}$ in a logical way decreases about 0 to 44% while the excentricity of the hyperellipsoid $S_{2,i}$ goes up from 0 to 85% . These results and other simulations allowed to get a qualitative appreciation of the relation between the TCP compliant displacements and the local stiffness variations. Moreover they validated the proposed local stiffness used to obtain a realistic description of the Surgiscope stiffness.

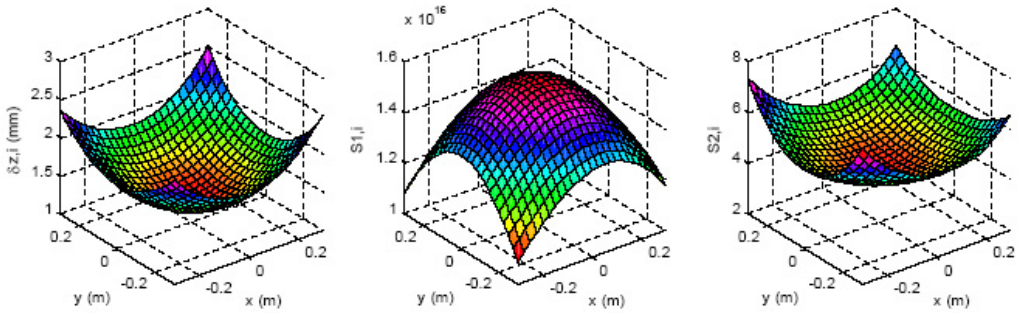

Fig. 5. δz_i, $S_{1,i}$ and $S_{2,i}$ for a 625 node planar grid set at the altitude $Z = -1.2\,m$.

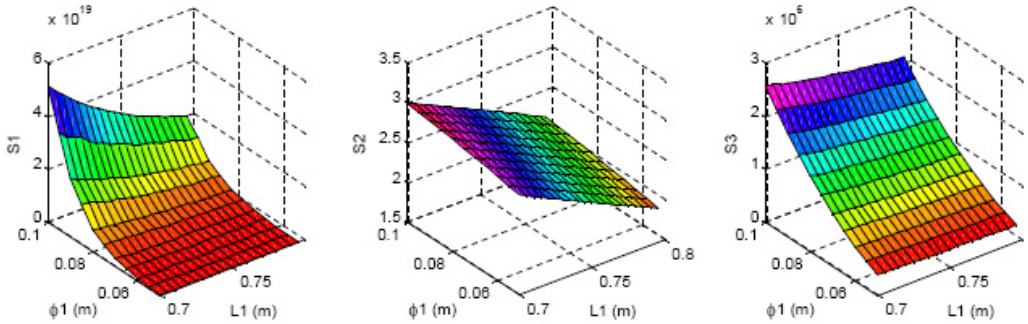

Fig. 6. Evolution of the global stiffness indices S_1, S_2 and S_3 under simultaneous variations of the geometrical parameters L_1 and ϕ_1.

TABLE II
DESIGN PARAMETERS VALUES

Parameters (Unit)	Nominal value	Lower bound	Upper bound	Step
$L_1\ (m)$	0.75	0.7	0.8	$1e^{-3}$
$L_2\ (m)$	0.95	0.85	1.05	$1e^{-3}$
$L_3\ (m)$	0.125	0.1	0.15	$1e^{-3}$
$T_1\ (mm)$	2	2	10	0.5
$T_2\ (mm)$	5	2	10	0.5
$\phi_1\ (mm)$	70	50	100	0.5
$\phi_2\ (mm)$	25	15	60	0.5
$\phi_3\ (mm)$	22	10	40	0.5
$R_n\ (m)$	0.2	0.15	0.25	$1e^{-3}$

C. Influence of the Surgiscope geometrical parameter variations onto the stiffness global indices

The main purpose of this part is to study the influence of the variations of the Surgiscope geometrical parameters onto its global stiffness (S_1, S_2 and S_3). This allows to verify that the variations of the global stiffness indices can describe the effects of the variations of the Surgiscope geometrical parameters. For this analysis, the spatial grid described in IV-A is used to calculate the global stiffness indices under the variations of the parameters given Table II.

For example, the Fig. 6 gives the results obtained for the simultaneous variations of the arm length L_1 and diameter ϕ_1 which values increase respectively from 0.7 to $0.8\,m$ and from 0.05 to $0.1\,m$. As one can see, the global stiffness of the Surgiscope decreases (see the variations of S_1 and S_3) for reduced values of L_1 when in the meantime it logically increases when the arm diameter ϕ_1 goes up.

To conclude this part, one can see that such parametric analyze is interesting at a pre-design stage to study the effects of one or two geometrical parameters onto the global stiffness of the Surgiscope. However, this analyze is limited since it is difficult to have a global overview of the combined effects of all geometrical parameters [25]. A solution of this problem is to achieve a multi-parameters and multi-criteria analyze as shown in the next part.

V. DESIGN OPTIMIZATION OF THE SURGISCOPE

A. Problem formulation

1) Design parameters: With reference to the Surgiscope mechanism under investigation, 9 design variables are tuned, which refer to the length, internal diameter and thickness of each bar constitutive of a kinematic chain, and also the radius of the moving platform R_n (Table. II). The radius of the base R_b is defined by the constraint relation $R = R_b - R_n$, with $R = 0.05\,m$.

Note that the genetic algorithm as optimization scheduler will imposed to considered the individual parameters such as discrete variables. The steps are defined by nearly respecting the manufacturing tolerances in order to not increase artificially the research space (Table. II).

2) Performances indices: As emphasized below, an optimal stiffness design of a robot manipulator can only be achieved by considering three global indices over the

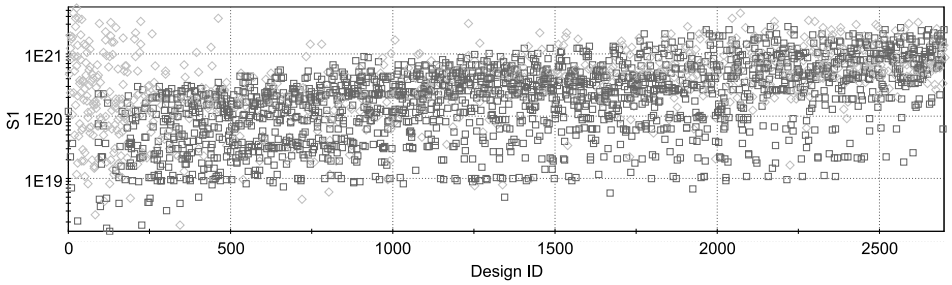

Fig. 7. Iteration history of S_1.

workspace. The objective of the optimization is to maximize both S_1 and S_3 while simultaneously minimizing S_2 to match values near to 1.

3) Constraints: In addition to these main performances indices, a constraint on the mass have to be set. The mass of the Surgiscope must not exceed the nominal threshold value of $21kg$. An indirect geometrical constraint is that all designs whose workspace does not include the nominal Surgiscope workspace defined in IV-A are automatically considered as invalid and excluded from the optimization flow.

B. Search method

1) Pareto-optimal solutions: Solving this optimization problem with multiple conflicting objectives across a high-dimensional design space is a difficult goal. Instead of a single optimum, there is rather a set of alternative trade-offs, generally known as Pareto-optimal solutions. Various evolutionary approaches to multi-objective optimization have been proposed since 1985, capable of searching for multiple Pareto-optimal solutions concurrently in a single simulation run [26]. The optimization program FRONTIER®[2] and the technical computing software MATLAB® are used to set up the framework of the multi-objective design optimization study of the Surgiscope. The Multi-objective Genetic Algorithm (MOGA), implemented first by Fonseca and Fleming [27], is used to perform the optimization problem.

2) Global optimization process: The algorithm will attempt a number of evaluations equal to the size of the initial population for the MOGA multiplied by the number of generation. A rule of thumb would suggest possibly to accumulate an initial population possibly more than $2 * number\ of\ variables * (number\ of\ objectives + number\ of\ constraints)$. Thus, the initial population is generated by a random sequence of 90 designs (9 design variables, 3 objectives, 1 constraint).

The major disadvantage of the MOGA is mainly related to the number of evaluations necessary to obtain satisfactory solutions. The search for the optimal solutions extends in all the directions from design space and produces a rich data base and there is not a true stop criterion. But the uniformity and the richness of the data base are very useful for the capitalization and the statistical analysis of the results. In the context of pre-stage design, the numerical evaluation of the performances calls upon MATLAB codes is not so expensive in terms of computing time (about $8\ s$). In an attempt to solve the optimization problem in an acceptable timeframe, the number of generations evaluated is almost 30, i.e. 2700 designs in all. The required computation time for the global optimization process is about 6 hours (2.0 GHz / 2.0 Gb RAM). Integrating a Response Surface Methodology to reduced the computation time could be an interesting extension of our work.

C. Numerical Results

1) Algorithm convergence: Fig. 7 highlights the MOGA convergence toward the maximization of the global index S_1. Of the 2700 designs analyzed, 8 generate an error since they do not respect the workspace required, and 759 are unfeasible designs since they do not respect the mass constraint fixed at $21\ kg$. These unfeasible designs are represented with a grey rhomb on Fig. 7. In spite of an initial population largely dominated by individuals exceeding the mass constraint, the algorithm allows a good and rather fast convergence.

Fig. 8 shows the projection of the resulting Pareto-optimal sets onto the S_1/S_2 domain, stressing the sensible improvement that can be obtained for the two objectives respecting

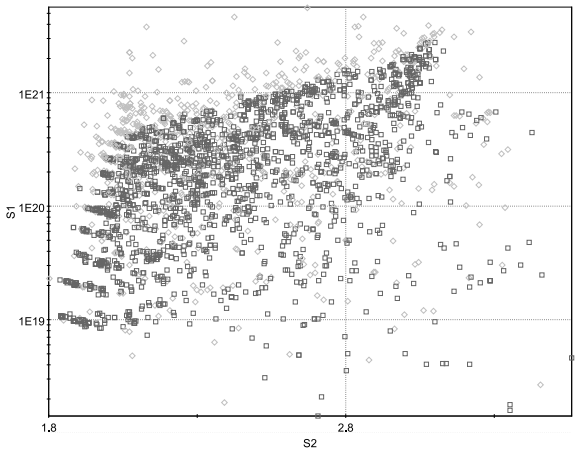

Fig. 8. Scatter chart of S_1 versus S_2.

[2]http://www.esteco.com/

the mass constraint. The most interesting characteristic of this figure is the shape of the Pareto-front on these objectives. The Pareto-front is very wide. This aspect indicates that there is a conflict between the objectives. The left-up region of the Fig. 8 is characterized by a non-feasibility against the mass constraint.

2) Tradeoffs decision using multiple criteria: The MOGA will by definition articulate design preference information after generating solutions. The MOGA defines a *posteriori* method which generates a set of solutions, with the decision marker's selecting a preferred solution afterwards. They can be regarded as a means of generating information for the user to base preference information on.

An ideal design would be one which gives the same objective function values as would be obtained if each objective were to be maximized on its own. Such a design is unlikely to exist. Rather, there will exist a set of best designs at the boundary of the feasible region. At any given point during an optimization, a set of feasible designs will have been evaluated. It may well not be known whether any of the designs is on or near the actual boundary of the feasible region. If the number is at all large, it will not even be obvious which of the designs are Pareto-optimal with respect to this particular set. So a filter needs to be provided to identify the non-dominated members of the set. These can then be listed numerically or displayed graphically. Various methods have been used to display sets of solutions in a multiple dimensional objective space. When there are many objectives and constraints, a main diagrammatic tool to assist understanding is parallel coordinates [28]. The selection of the optimal structure inside the Pareto-set designs can be done easily by using an interactive filter on the parallel coordinates chart of the global stiffness indices and the mass constraint (Fig. 9). The design engineer balances these factors off against each others to arrive at what he thinks is the best combination of properties in the final design. There's no a unique solution. It is clear that in broad terms design is a creative process involving the use of knowledge and experience of the designer.

3) Optimal stiffness design: Of the 2700 designs analyzed, 69 were Pareto-optimal with respect to the others. Of these, the design ID 1964 is identified as being a good candidate for best overall design. The improvement of the optimal stiffness solution with respect to the nominal design is discussed in detail and shown in Table. III. The comparison of the stiffness performances of the candidate optimal solution with those of the nominal structure stresses the sensible improvement that can be obtained for all the

TABLE III

EVALUATION GLOBAL STIFFNESS INDICES FOR THE SURGISCOPE

Design	Mass (kg)	S_1	S_2	S_3
Nominal	20.2	$1.99e20$	2.79	$4.21e6$
ID 2556	20.2	$6.53e20$	2.37	$6.49e6$
ID 1188	16.7	$2.04e20$	2.43	$4.37e6$

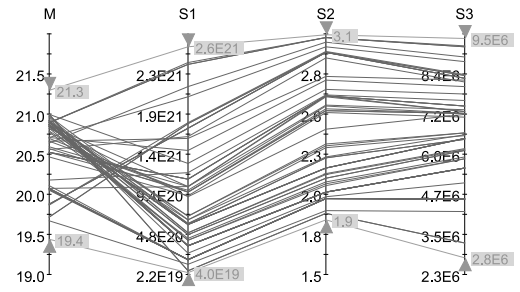

Fig. 9. Parallel coordinates chart of the Pareto-optimal designs.

objectives with an identical mass. The average improvement on the global stiffness performance indices S_1 and S_3 is about 65% while the performance index S_2 prove to be 15% better than the corresponding of the reference structure. Design characteristics for the optimum solution are reported in Table. IV. The geometrical modifications obtained for the optimal design ID 2556 confirm the conclusions advanced in IV-C.

In order to show the stiffness improvement, we have computed the value of the maximal and the mean of the resulting TCP elastic displacements for a payload of $800N$ (Table. V). By considering the optimal stiffness design ID 2556, the improvement is about 30% on the mean as on the max of the resulting TCP elastic displacement δz_i. Even if the global optimization indices relate only to the translational stiffness matrix $\mathbf{K}^t_{eq,i}$, the angular deflections are also optimized in almost the same proportion that those in translation for the design ID 2556 (Table. V). Fig. 10 illustrates the distribution of the resulting TCP elastic displacements δz_i at the altitude $Z = -1.2\,m$ for the optimal and nominal designs. It can be observed that the improvement obtained for the design ID 2556 is uniformed all over the workspace, and note that the excentricity is also reduced.

4) Optimal weight design: The search for the optimal stiffness provides solutions that preserve identical stiffness properties to the nominal design, while minimizing the mass. The design ID 1188 performs a reduction of almost 20% on the mass while conserving, or even while improving global stiffness indices (Table. III).

TABLE IV

DESIGN CHARACTERISTICS OF OPTIMAL SOLUTIONS.

Parameters (Unit)	Nominal	ID 2556	ID 1188
$L_1\ (m)$	0.75	0.773	0.762
$L_2\ (m)$	0.95	0.917	0.954
$L_3\ (m)$	0.125	0.106	0.112
$T_1\ (mm)$	2	7	5
$T_2\ (mm)$	5	2	2
$\phi_1\ (mm)$	70	74	70
$\phi_2\ (mm)$	25	17.5	23
$\phi_3\ (mm)$	22	23.5	21
$R_n\ (m)$	0.2	0.152	0.151

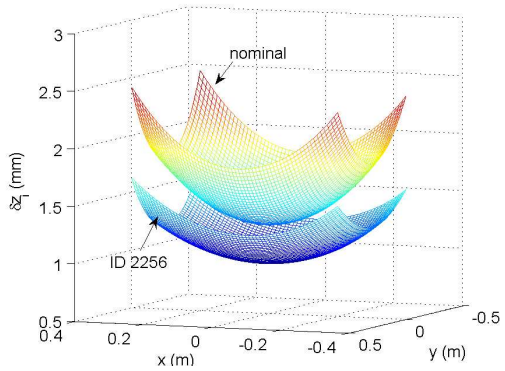

Fig. 10. δz_i for a 625 node planar grid set at the altitude $Z = -1.2\,m$.

TABLE V

MEAN AND MAXIMUM OF THE TCP ELASTIC DISPLACEMENTS.

Design	$\delta x_i(mm)$		$\delta y_i(mm)$		$\delta z_i(mm)$	
	mean	max	mean	max	mean	max
Nominal	-0.006	2.27	0.0	3.93	1.80	3.17
ID 2556	-0.007	1.36	0.0	2.53	1.26	2.25
ID 1188	-0.006	1.87	0.0	3.25	1.75	2.80
Design	$\delta\theta x_i(mrad)$		$\delta\theta y_i(mrad)$		$\delta\theta z_i(mrad)$	
	mean	max	mean	max	mean	max
Nominal	0.0	8.86	-0.01	6.79	0.0	0.42
ID 2556	0.0	7.75	-0.01	5.40	0.0	0.39
ID 1188	0.0	8.28	-0.01	6.09	0.0	0.36

VI. CONCLUSION

Design optimization of robots manipulators must be done in a short period of time and, as a result, an automated procedure for finding an optimum stiffness structure is proposed. The presented optimization, based on an original and systematic elasto-geometrical modeling, fulfills the industrial demands in the preliminary design of the robot manipulators: optimizing simultaneously the stiffness over a specific workspace and minimizing the global weight of the structure for dynamic performances increased, the whole in an acceptable timeframe. The interactive use of evolutionary multi-objective algorithm in the robot design optimization is very attractive from the engineering viewpoint. Pareto-optimization may be considered as a tool providing a set of efficient solutions among different and conflicting objectives, under different constraints. The final choice remains always subjective and is left to the designer responsibility.

REFERENCES

[1] L.-W. Tsai. *Robot Analysis, the Mechanics of Serial and Parallel Manipulator*. John Wiley & Sons, Inc., 1999.

[2] J. Duffy. *Statics and Kinematics with Applications to Rob.* Cambridge University Press, 1996.

[3] K. Schroer, S. L. Albright, and A. Lisounkin. Modeling closed-loop mech.s in robots for purposes of calibration. *IEEE Trans. on Rob. and Aut.*, 13(2):218–229, 1997.

[4] M Damak and J Grosbois. Vision robot based absolute accuracy measurement. In *ISR 2004*, Paris, France, 2004.

[5] G. Alici and B. Shirinzadeh. Enhanced stiffness modeling, identification and characterization for robot manipulators. *IEEE Trans. on Rob. and Aut.*, 21(4):554–564, 2005. 1552-3098.

[6] S. Marie and P. Maurine. Elasto-geometrical modelling of closed-loop industrial robots used for machining applications. In *IEEE Int.Conf. on Rob. and Aut., 2008*, pages 1294–1300, 2008.

[7] G. Carbone and M. Ceccarelli. A comparison of indices for stiffness performance evaluation. In *IFToMM'07*, Besançon, France, 2007.

[8] C. Gosselin and SA INRIA. Stiffness mapping for parallel manipulators. *IEEE Trans. on Rob. and Aut.*, 6:377–382, 1990.

[9] G. J. Wiens and D. S. Hardage. Structural dynamics and system identification of parallel kinematic machines.

[10] M. Krefft and J. Hesselbach. Elastodynamic optimization of parallel kinematics. *IEEE Int. Conf. on Aut. Science and Engineering*, pages 357–362, 2005.

[11] S. D. Stan, V. Maties, and R. Balan. Genetic algorithms multiobjective optimization of a 2 dof micro parallel robot. *IEEE Conf. on Emerging Technologies & Factory Aut.*, pages 780–783, 2007.

[12] R. Unal, G. Kiziltas, and V. Patoglu. A multi-criteria design optimization framework for haptic interfaces. *Symposium on Haptic Interfaces for Virtual Environment and Teleoperator Systems*, pages 231–238, 2008.

[13] D. Deblaise, X. Hernot, and P. Maurine. A systematic analytical method for pkm stiffness matrix calculation. In *IEEE Int. Conf. on Rob. and Aut.*, pages 4213 – 4219, Orlando, Floride, USA, 2006.

[14] J. P. Merlet. Jacobian, manipulability, condition number, and accuracy of parallel robots. *Journal of Mechanical Design*, 128:199–206, 2006.

[15] R. Clavel. Delta, a fast robot with parallel geometry. In *18th Int. Symp. Ind. Robots*, pages 91–100, Lausanne, Switzerland, Apr. 1988.

[16] J.H. Borm and C.H. Menq. Experimental study of observability of parameter errors in robot calibration. In *The IEEE Int. Conf. on Rob. and Aut.*, volume 1, pages 587–591, Scottsdale, Arizona, USA, 1989.

[17] B. Mooring, Z. Roth, and Driels M. *Fundamentals of manipulator calibration*. John Wiley and Sons Inc, New York, 1991.

[18] A.N. Nahvi, J. M. Hollerbach, and V. Hayward. Calibration of a parallel robot using multiple kinematic closed loops. In *The IEEE Int.Conf. on Rob. and Aut.*, volume 1, pages 142–148, San Diego, USA, 1994.

[19] A.N. Nahvi and J. M. Hollerbach. The noise amplification index for optimal pose selection in robot calibration. In *The IEEE Int. Conf. on Rob. and Aut.*, pages 647–654, Minneapolis, Minnesota, USA, 1996.

[20] Y. Sun and J. M. Hollerbach. Observability index selection for robot calibration. In *The IEEE Int. Conf. on Rob. and Aut., 2008. ICRA 2008*, pages 831–836, Pasadena, California, USA, 2008.

[21] C. H. Menq and J. H. Borm. Statistical measure and characterization of robot errors. In *The IEEE Int. Conf. on Rob. & Aut.*, volume 2, pages 926–931, Philadelphia, PA, 1988.

[22] O. Ma and J. Angeles. Optimum architecture design of platform manipulators. In *ICAR., Fifth Int. Conf. on Advanced Rob.*, pages 1130–1135 vol.2, 1991.

[23] SG. Kim and J. Ryu. New dimensionally homogeneous jacobian matrix formulation by three end-effector points for optimal design of parallel manipulators. *IEEE Trans. on Rob. and Aut.,*, 19(4):731–736, 2003. 1042-296X.

[24] Raffaele Di Gregorio. Determination of singularities in delta-like manipulators. *The Int. Journal of Rob. Research*, 23:89–96, 2004.

[25] F. Majou, C. Gosselin, P. Wenger, and D. Chablat. Parametric stiffness analysis of the orthoglide. *Mechanism and Machine Theory*, 42:296–311, 2007.

[26] D. A. V. Veldhuizen and G. B. Lamont. Multiobjective evolutionary algorithms: Analyzing the state-of-the-art. *Evolutionary Computation*, 8:125–147, 2000.

[27] C. M. Fonseca and P. J. Fleming. Multiobjective optimization and multiple constraint handling with evolutionary algorithms. *IEEE Trans. on Systems, Man, and Cybernetics*, 28:26–37, 1998.

[28] A. Inselberg, B. Dimsdale, IBMS Center, and C. A. Los Angeles. Parallel coordinates: a tool for visualizing multi-dimensionalgeometry. *IEEE Conf. on Visualization*, pages 361–378, 1990.